Journal of Thermal Analysis and Calorimetry, Vol. 91 (2008) 3, 879–884

CRYSTALLIZATION KINETICS AND THERMAL STABILITY OF AN AMORPHOUS $Fe_{77}C_5B_4Al_2GaP_9Si_2$ BULK METALLIC GLASS

Á. Révész[*]

Department of Materials Physics, Eötvös University. H-1518 Budapest, P.O.B. 32, Hungary

The thermal stability, kinetics and glass forming ability of an $Fe_{77}C_5B_4Al_2GaP_9Si_2$ bulk amorphous alloy have been studied by differential scanning calorimetry. The activation energy, frequency factor and rate constant corresponding to the multiple crystallization steps were determined by the Kissinger method. X-ray diffraction and transmission electron microscopy studies revealed that the crystallization starts with the primary precipitation of α-Fe from the amorphous matrix. The kinetics of nucleation of the α-Fe nanoparticles was investigated by two different methods, i.e. isothermal annealing and continuous heating after partial annealing.

Keywords: *bulk metallic glass, Fe-based, kinetics, nucleation*

Introduction

Bulk metallic glasses (BMGs) constitute a novel and exciting class of metallic materials with unique properties for structural and functional applications. Among them, iron-based metallic glasses are particularly important due to their excellent magnetic and mechanical properties [1, 2]. Previously, amorphous ferromagnetic alloys were developed for potential use as electrical transformers, motors, magnetic sensors, switching power supplies and other electrical energy conversion devices [3], nevertheless, all these alloys were inevitably produced by quenching the melt at a cooling rate of the order of 10^6 K s^{-1} and as a result ribbons, films or wires were fabricated, which largely restrains the commercial applications. On the other hand, the investigation of the thermal stability and crystallization of rapidly quenched Fe-based metallic glasses [4–7] is of great importance in order to increase sample dimensions. In the last years, therefore, significant efforts have been made to improve the glass forming ability (GFA) combined with excellent soft magnetic properties of ferrous BMGs [8–10]. Recently, much attention has been paid to the development of a new class of Fe-based BMGs with very high Curie-temperature for high temperature magnetic applications [11].

In order to better characterize the optimum annealing treatment of ferromagnetic metallic glasses, it is necessary to study the glass-transition and crystallization kinetics in detail. In the following paper the thermal stability, GFA and crystallization behavior during continuous heating and isothermal annealing of $Fe_{77}C_5B_4Al_2GaP_9Si_2$ bulk metallic glass with a diameter of 3 mm will be discussed.

Experimental

Multicomponent master alloy with a composition of $Fe_{77}C_5B_4Al_2GaP_9Si_2$ was prepared by arc melting under Ti-gettered Ar atmosphere. The rod shape specimen with a diameter of 3 mm was prepared by injecting the molten alloy into the cylinder-shaped cavity of a copper mold.

Differential scanning calorimetry (DSC) experiments were carried out in a Perkin-Elmer power compensated device under a pure dynamic argon atmosphere. Continuous heating studies were performed at scan rates in the range of 2.5–80 K min^{-1}. The transformation enthalpies were obtained as the area of the exothermic peaks. Isothermal heat treatments were carried out by heating the samples to the heat-treatment temperature at a rate of 100 K min^{-1}. Each measurement was followed by a second scan to obtain the baseline. From the shift of the DSC peaks with increasing heating rate, the apparent activation energy of the crystallization processes was determined [12]. High temperature behavior was examined by a Setaram Differential Thermal Analyzer (DTA) at heating rate of 20 K min^{-1}.

The microstructure of the as-cast and annealed alloys was examined by X-ray diffraction (XRD) using Cu-K_α radiation on a Philips X'pert powder diffractometer in θ–2θ geometry. The average crystalline sizes of the heat-treated samples were determined by the Scherrer formula [13].

Transmission electron microscopy (TEM) was carried out using a Phillips CM30 electron microscope operated at 300 keV. For TEM observations the samples were mounted on a copper grid and ion thinned.

* reveszadam@ludens.elte.hu

1388–6150/$20.00

Akadémiai Kiadó, Budapest, Hungary
Springer, Dordrecht, The Netherlands

Results and discussion

Continuous heating

The GFA and thermal stability of the as-cast $Fe_{77}C_5B_4Al_2GaP_9Si_2$ alloy were examined by continuous heating DSC experiments, as seen in Fig. 1. At all heating rates these curves present a distinct glass-transition (T_g) followed by a supercooled liquid region ($\Delta T_x=T_{on}-T_g$) and then by three overlapping exothermic crystallization peaks (T_{px}, T_x, T_{hx}). Increasing heating rate results in higher T_g, T_{px}, T_x and T_{hx} (Table 1). As seen the ΔT_x region is as wide as 40 K (at 20 K min^{-1} of heating rate) indicating the high resistance of the undercooled liquid to crystallization and consequently the nucleation of any primary crystalline phase is retarded. It is noted the ΔT_x depends not just on the heating rate, but on the applied pressure as well [14]. The estimated values of ΔH_{px}, ΔH_x and ΔH_{hx} were 31, 82 and 25 J g^{-1}, respectively and are practically independent from the applied heating rate. The liquidus temperature determined from the high temperature DTA curve (see the inset) was 1252 K. The calculated T_r reduced glass transition (0.59) also refers to an excellent glass former.

Figure 2 focuses on the shift of the glass transition region with heating rate. This amorphous-to-supercooled liquid transition phenomenon can be described by using two different approaches. Some reports have calorimetrically observed a linear increase of T_g with the logarithm of the heating rate, β:

$$T_g=T_0+U\ln\beta \quad (1)$$

where T_0 and U are constants [15]. However, there are also investigations which reveal a Vogel–Fulcher–Tammann (VFT)-type of behavior for describing the variation of T_g as a function of β [16]:

$$\beta=B\exp\left(\frac{A}{T_g^0-T_g}\right) \quad (2)$$

or

$$T_g=T_g^0+\frac{A}{\ln\left(\frac{B}{\beta}\right)} \quad (3)$$

where A and B are constants and T_g^0 is the asymptotic value of T_g usually approximated as the onset of the glass transition in the limit of infinitely slow cooling rate. It should be mentioned that explicit fitting of the DSC data by the three parameters of Eq. (2) is not possible, an evaluation of T_g^0 from viscosity measurements at different temperatures [17, 18] followed by fitting the remaining two VFT parameters is necessary. Nevertheless, as seen in the inset of Fig. 2, the experimental data points well follows the Lasochka's linear relationship, the obtained fitting parameters are: T_0=722 K and U=8.85, in accordance with the values corresponding to Zr-based BMGs [19].

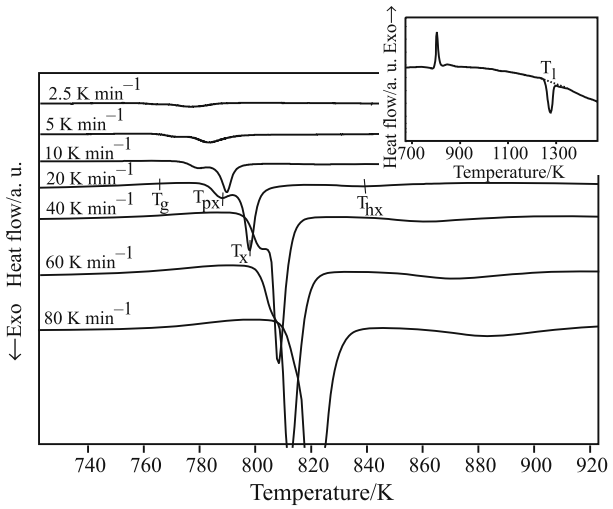

Fig. 1 Continuous heating DSC curves obtained at different heating rates. The inset shows the high temperature DTA plot

Table 1 Phase transformation parameters obtained from the continuous heating experiments for the $Fe_{77}C_5B_4Al_2GaP_9Si_2$ bulk metallic glass

β/K min^{-1}	T_g/K	T_{on}/K	T_{px}/K	T_x/K	T_{hx}/K	ΔT_x/K
2.5	–	759	765	780	–	–
5	733	765	772	786	–	32
10	736	772	778	792	822	36
20	739	780	785	799	836	40
40	738	786	792	805	852	48
60	743	789	800	808	596	45
80	749	792	800	812	869	43

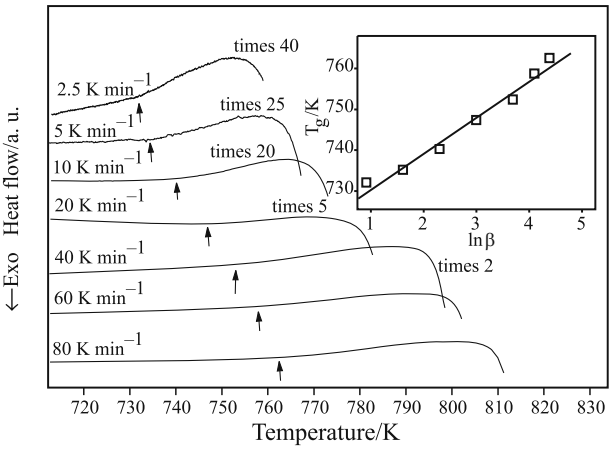

Fig. 2 Linear heating DSC curves showing the shift of the glass transition with increasing heating rate. The inset shows the dependence of the glass transition temperature *vs*. the logarithm of the heating rate

Based on these results, the glass transition process can be regarded as a kinetically modified thermodynamic phase transformation.

The activation energy (E_a) and the frequency factor (Z) corresponding to glass transition and individual crystallization steps are estimated from the Kissinger method [12]. The dependence of peak temperatures (T_g, T_{px}, T_x, T_{hx}) on the heating rate can be given by the

$$\frac{\beta}{T_i^2}=\frac{Z_i R}{E_{a,i}}\exp\left(\frac{-E_{a,i}}{RT_i}\right) \quad (4)$$

equation, where R is the gas constant and the index i refers to g, px, x or hx. Plotting $\ln(\beta/T_i)$ *vs.* T_i^{-1} enables the independent determination of $E_{a,i}$ for each step from the slope of the fitted straight line (Fig. 3). The calculated values ($E_{a,g}$=7.2 eV at^{-1}, $E_{a,px}$=5.2 eV at^{-1}, $E_{a,x}$=5.8 eV/atom and $E_{a,hx}$=2.5 eV at^{-1}) are considerably large indicating high thermal stability and suggest that the crystallization takes place through a nucleation and growth process [20]. The frequency factor, which measures the probability that an atom having energy E_a joins an existing nucleus, can be determined from the intercept of the fitted line with the ordinate, the obtained values ($Z_{px}=2.7\cdot10^{25}$ s^{-1} and $Z_x=9.4\cdot10^{28}$ s^{-1}) similar to those for other Fe-based BMG [21]. The temperature dependence of the rate constant, k_{cr} follows the Arrhenius-type of relationship

$$k_{cr}(T)=Z\exp\left(\frac{-E_{a,i}}{RT}\right) \quad (5)$$

as seen on the monotonously increasing curves in the inset of Fig. 3 for the first two exothermic transformations. To some extent, k_{cr} can be correlated with the GFA, i.e. a BMG with smaller k_{cr} is a better glass-former [19].

The evolution of the microstructure during the crystallization process can be followed on the XRD patterns of the $Fe_{77}C_5B_4Al_2GaP_9Si_2$ BMG in Fig. 4. As seen the as-cast state exhibits a broad and symmetric halos around 2θ=45 and 80° without any sharp diffraction peaks, which is typical for a fully amorphous phase. The corresponding selected are electron diffraction pattern (SAED), see Fig. 5a, consists of halo rings and the bright-field electron micrograph (not shown) reveals featureless contrast, indicating the absence of any crystallinity in the as-cast state.

After the first crystallization stage (linear heating at 20 K min^{-1} up to 785 K), the XRD pattern still indicates a strong amorphous halo with a crystalline peak of α-Fe. These primary crystallites are homogeneously dispersed in the residual amorphous matrix and the average crystallite-size after the first stage was found to be 17±2 nm. Above 800 K the spectrum indicates that the material is almost fully crystalline containing multiple phases, i.e. α-Fe, Fe_3B, Fe_3P, Fe_3C and Fe_2B. The 3rd crystallization stage (873 K) results in only sharper Bragg-peaks corresponding to some grain-growth. The final grain size for the α-Fe crystallites is 42±4 nm. The corresponding SAED pattern shows that several phases formed (Fig. 5b), however, their identification leads to the same difficulty as for the XRD data. The TEM micrograph gives a direct imaging of the microstructure, the arrangement of crystallites is homogenous without any amorphous background (Fig. 5c).

Isothermal behavior

Isothermal annealing of the as-cast $Fe_{77}C_5B_4Al_2GaP_9Si_2$ alloy was carried out in order to study the crystalliza-

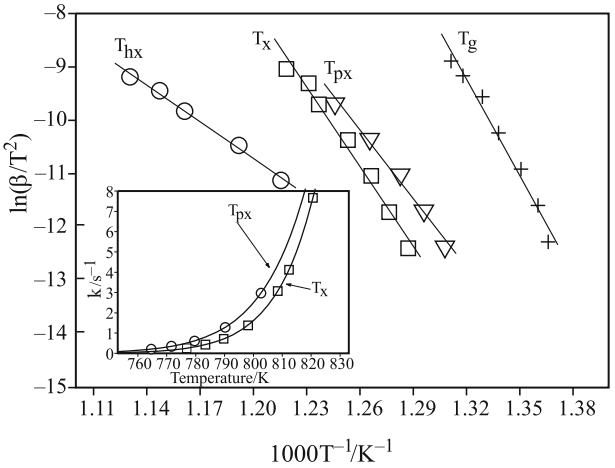

Fig. 3 Kissinger plots obtained from the shift of the transformation peak temperatures as a function of heating rate. The inset shows the temperature dependence of the rate constant

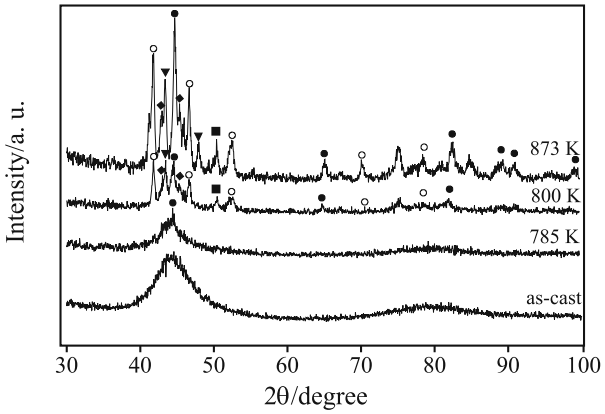

Fig. 4 XRD patterns corresponding to the as-cast, partially crystallized (continuous heating at 20 K min^{-1} up to 785 and 800 K) and fully crystalline states of the $Fe_{77}C_5B_4Al_2GaP_9Si_2$ alloy. The symbols denote the Bragg-peaks: ● – α-Fe, ▼– Fe_3B, ○– Fe_3P, ◆ – Fe_3C and ■ – Fe_2B, respectively

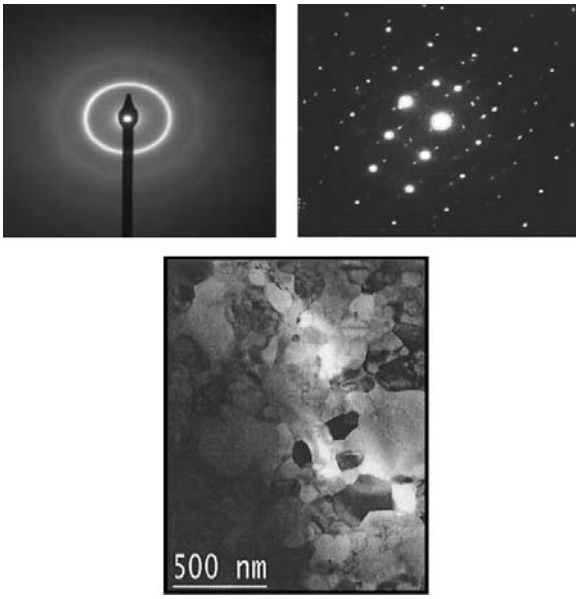

Fig. 5 SAED patterns of the a – as-cast and b – fully crystallized states. The bright field image corresponds to the c – fully crystallized state

tion mechanism in detail. Figure 6 depicts the isothermal DSC measurements carried out at different T_{ann} annealing temperatures in the range of 761–768 K for 60 min. As seen, each isotherm has two distinct exothermic peaks which can correlate with the T_{px} and T_x crystallization steps in the continuous DSC curves (Fig. 1), indicating that the crystallization process occurs through a nucleation and growth mechanism [22]. With increasing T_{ann}, the peak maxima (t_{px} and t_x) occur at shorter times, from the slope of the $\ln(t_p)$ *vs*. T_{ann}^{-1} function (Fig. 7) the apparent activation energies were determined: $E_{a,px}^{iso}$=5.3 eV and $E_{a,x}^{iso}$=5.5 eV. The similar values obtained for the first and second crystallization peak from the continuous heating indicate that the atoms participating in the nucleation during both isothermal and non-isothermal treatments acquire, on average, similar amount of energy to form an activated crystalline cluster.

Figure 8 shows the DSC curves obtained during continuous heating (20 K min^{-1}) of the as-cast alloy after annealing at 761 K for different times (2, 5, 10 and 60 min). As seen, the first exothermic peak (which corresponds to the primary precipitation of α-Fe) gradually diminishes up to 10 min of annealing, while the area of the second peak remains practically unchanged. Longer annealing (60 min) will lead to the completion of the second crystallization step as well. In accordance, the corresponding XRD patterns taken after annealing at 761 K for different times show the development of only α-Fe up to 10 min (Fig. 9). 15 min of annealing results in the joint formation of Fe_3B, Fe_3P and Fe_3C, while after 25 min of annealing (appr. the time of completion of the

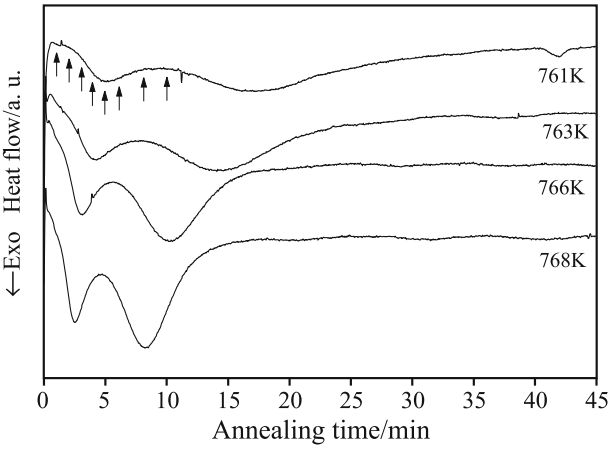

Fig. 6 Isothermal DSC curves of the amorphous $Fe_{77}C_5B_4Al_2GaP_9Si_2$ alloy obtained at different annealing temperatures. The arrows indicate the length of the pre-anneals at T_{ann}=761 K

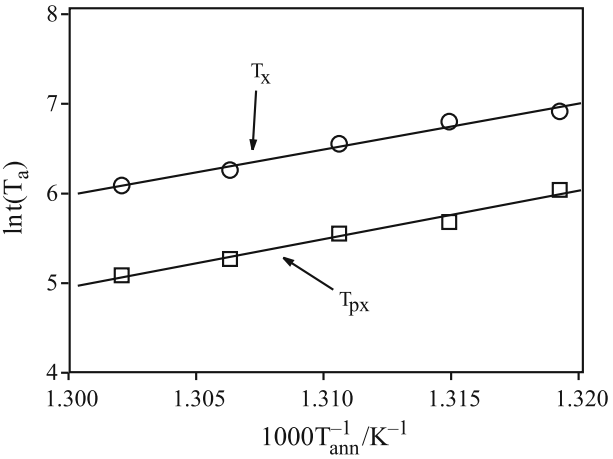

Fig. 7 The logarithm of isothermal peak positions as a function of the inverse temperature

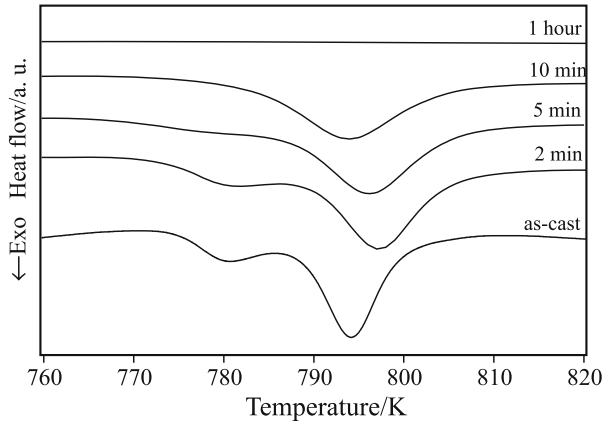

Fig. 8 Continuous heating DSC curves obtained after pre-anneals for different times at T_{ann}=761 K

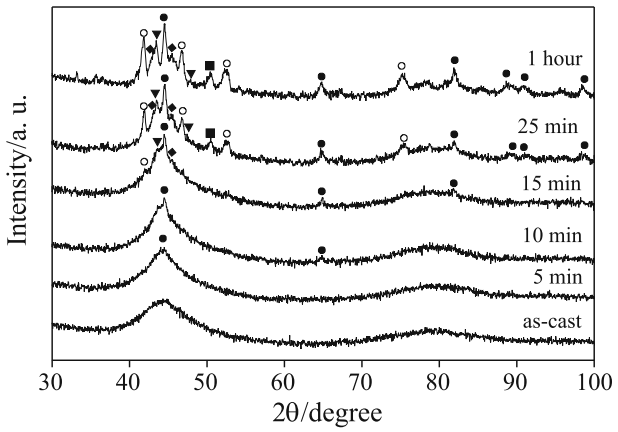

Fig. 9 XRD patterns corresponding to the pre-annealed samples for different times at T_{ann}=761 K. The symbols denote the Bragg-peaks: ● – α-Fe, ▼ – Fe_3B, ○ – Fe_3P, ◆ – Fe_3C and ■ – Fe_2B, respectively

second reaction) the Fe_2B peaks also appear. Longer annealing does not change the pattern significantly.

Kinetics of crystallization

Generally, the crystallization kinetics can be studied either by isothermal annealing experiments or by continuous DSC after partial isothermal annealings (pre-anneals). In the first case the transformed volume fraction corresponding to a single reaction can be evaluated from the measured isothermal heat flow signal after baseline substraction and, if necessary, peak deconvolution.

Figure 10 shows the crystalline transformed fraction curve (solid line) of the α-Fe phase at 761 K obtained directly from the isothermal measurement according to the following equation

$$x(t)=\frac{\int_0^t \dot{H}_1^{iso}(t')\mathrm{d}t'}{\Delta H_1^{iso}} \quad (6)$$

where $x(t)$ is the transformed fraction, $\dot{H}_1^{iso}$ is the measured heat flow at time t' and ΔH_1^{iso} the total enthalpy of the first crystallization stage during the isothermal annealing. Note that increasing the annealing temperature, the transformation is completed in shorter times. In the classical nucleation theory the Johnson–Mehl–Avrami equation [23],

$$x(t)=1-\exp[-(K(T)t)^n] \quad (7)$$

describes the fraction of the transformed material in an isothermal process, where $K(T)$ is a temperature dependent kinetic constant and n is the Avrami exponent which varies between 0.5 and 4 depending on the nature of the nucleation and growth mechanism. Assuming that n is constant during the whole

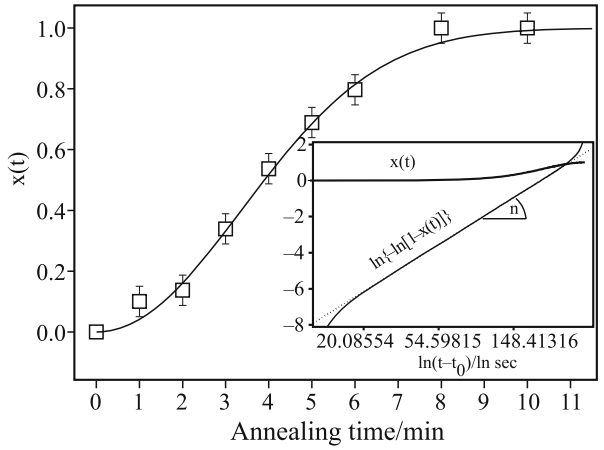

Fig. 10 Isothermal transformation curve corresponding to the primary precipitation of α-Fe from the amorphous matrix. The JMA fit gives n=2.1. The squares denote the values determined from continuous heating DSC curves following pre-anneals at T_{ann}=761 K

reaction, the $\ln\{-\ln[1-x(t)]\}$ *vs.* $\ln(t-t_0)$ plot should give a straight line with a slope equal to n, where t_0 is an incubation time. As seen in the inset of Fig. 10 the function obtained from the measured isothermal DSC curve well follows the linearity in a wide time interval. The calculated Avrami exponent (n=2.1) indicates that nucleation and diffusion controlled growth process takes place during the nucleation of α-Fe nanoclusters from the amorphous matrix [24].

In the second approach it is assumed that the total enthalpy release (during the pre-anneal and during the continuous scan) is constant, the transformed crystalline fraction in the pre-anneal can be evaluated by measuring the residual area of the first crystallization peak in the continuous DSC curves obtained after the pre-anneals. The transformed volume fraction can then be calculated as:

$$x(t)=\frac{\Delta H_1-\Delta H_1(t)}{\Delta H_1} \quad (8)$$

where $\Delta H_1(t)$ is the measured enthalpy release of the first reaction during the continuous heating after the pre-anneal of a period, t. The length of the pre-anneals is marked by arrows in Fig. 6. Such continuous scans after pre-anneals have already been shown in Fig. 8. The calculated $x(t)$ values according to Eq. (8) are marked by empty squares in Fig. 10. As seen these data points fit very well onto the $x(t)$ curve obtained from isothermal DSC experiments, indicating that both procedures are valid for determining the transformed crystalline fraction and the nature of nucleation and growth.

Conclusions

The $Fe_{77}C_5B_4Al_2GaP_9Si_2$ bulk metallic glass with a diameter of 3 mm exhibits a combination of excellent GFA parameters: T_g=739 K, ΔT_x=40 K, T_r=0.59. The high activation energy value of the first crystallization step corresponds to high thermal stability. During the first exothermic reaction, primary precipitation of α-Fe nanocrystals takes place, while at higher temperatures the remaining amorphous matrix transforms into multiple crystalline phases. The kinetics of nucleation of the α-Fe nanoparticles was investigated by two different methods: isothermal annealing and continuous heating after partial pre-anneals. Both approaches confirmed that nucleation and diffusion controlled growth process takes place during the nucleation of α-Fe nanoclusters.

Acknowledgements

The author acknowledges the financial support of the Hungarian Scientific Research Fund (OTKA) under grant 67893 and the Bolyai Post Doctoral Fellowship of the Hungarian Academy of Sciences.

References

1 T. Mizushima, A. Makino, S. Yoshida and A. Inoue, J. Appl. Phys., 85 (1999) 4418.
2 E. Jartych, K. Pekala, P. Jaskiewicz, J. Latuch, M. Pekala and J. Grabski, J. Alloys Compd., 343 (2002) 211.
3 D. Raskin and C.H. Smith, Amorphous Metallic Alloys, F. E. Luborsky, Ed., Butterworths, London, 1983.
4 T. Spassov and S. Budurov, J. Thermal Anal., 45 (1995) 1557.
5 P. Šimon, E. Illeková and S. C. Mojumdar, J. Therm. Anal. Cal., 83 (2006) 67.
6 J. J. Suńol, M. T. Clavaguera-Mora and N. Clavaguera, J. Therm. Anal. Cal., 72 (2003) 347.
7 D. C. Ile, Á. Révész, H. Grahl, J. Eckert, P. Crespo, P. Marín, A. Hernando, S. Surinach, J. S. Munoz and M. D. Baró, Mater. Sci. Eng. A, 375–377 (2004) 297.
8 K. Ikarashi, T. Mizushima, A. Makino and A. Inoue, Mater. Sci. Eng. A, 304–306 (2001) 763.
9 V. Ponnambalam, S. J. Poon and G. J. Shiflet, J. Mater. Res., 19 (2004) 1320.
10 Z. P. Lu, C. T. Liu, C. A. Carmichael and W. D. Porter, J. Mater. Res., 19 (2004) 921.
11 H. Y. Kim, J. Mater. Sci., 42 (2007) 2675.
12 H. E. Kissinger, Anal. Chem., 29 (1957) 1702.
13 H. P. Klug and L. E. Alexander, X-ray Diffraction Procedures for Polycrystalline and Amorphous Materials, Wiley, New York 1974.
14 J. Z. Jiang, J. S. Olsen, L. Gerward, S. Abdali, J. Eckert, N. Schlorke-de Boer, L. Schultz, J. Truckenbrodt and P. X. Shi, J. Appl. Phys., 87 (2000) 2664.
15 M. Lasocka, Mater. Sci. Eng., 23 (1976) 173.
16 R. Brüning and K. Samwer, Phys. Rev. B, 46 (1992) 11318.
17 F. Chen, C. Tsin and S. Zhou, Mater. Sci. Eng. A, 373 (2004) 158.
18 R. Busch, E. Bakke and W. L. Johnson, Acta Mater., 46 (1998) 4725.
19 Y. X. Zhuang, W. H. Wang, Y. Zhang, M. X. Pan and D. Q. Zhao, Appl. Phys. Lett., 75 (1999) 2392.
20 A. Inoue, K. Nakazato, Y. Kawamura, A. P. Tsai and T. Masumoto, Mater. Trans. JIM, 35 (1994) 102.
21 N. Mitrovic, S. Roth and J. Eckert, Appl. Phys. Lett., 78 (2001) 2145.
22 L. C. Chen and F. Spaepen, Nature, 336 (1988) 366
23 M. Avrami, J. Chem. Phys., 9 (1941) 177.
24 J. W. Christian, The Theory of Transformations in Metals and Alloys, 2nd Ed., Pergamon, Oxford 1975.

Received: July 11, 2007
Accepted: September 12, 2007

DOI: 10.1007/s10973-007-8632-4